The University of Alabama in Huntsville

Final Research Report

SPECTROSCOPIC STUDY OF COMBUSTION DIAGNOSTICS ON HYDROXYL RADICALS

Prepared by

R. J. Hung

The University of Alabama in Huntsville

Huntsville, Alabama 35899

NASA Grant: NAG8-102

Abstract

Experimental observations of propane/air flames have been carried out. Measurements of hydroxyl (OH) radical concentration have been made using resonance line absorption techniques. A microwave-pumped low pressure discharge in argon and water vapor is employed to produce strong OH radical band radiation in the 308 nm region. This radiation is transmitted through the plume and absorption data are taken at various radial positions using an optical multichannel analyzer. This absorption data is used to compute OH number density using a model for the absorption band characteristics as a function of temperature based on an atlas of line strengths. A numerical computation of flow fields, temperature profile and OH number density is carried out by using a technique of computational fluid dynamics (CFD). The results of CFD computation are compared with experimental observation with a good agreement.

I. Introduction

Experimental observations of propane/air flames have been conducted. These measurements have been made as a part of a program for the characterization of rocket engine exit plane properties for performance code validation. The rocket engines of interest are liquid oxygen/liquid hydrocarbon fueled. The major species resident in the exhaust of these engines include H_2O, CO_2, CO, OH and H_2. In this study, the primary effort has been concerned with the determination of the OH radical based on spectroscopic techniques. A numerical calculation based on fluid dynamics and combustion code has been carried out to compute OH radical distribution, temperature profile and flow field which were compared with experimental results.

The present study is based on the absorption of ultraviolet radiation by OH radicals in combustion systems. The concept of the measurement is based on the assumption that the medium in question is in vibrational and rotational equilibrium. Gaydon [1] describes several similar techniques. Neer [2] first described the application of this technique to high speed flows using a rapidly scanning single channel monochromator. In this paper, the measurement is based upon differential absorption of radiation associated with the $2\Sigma^+ - 2\pi$ band which occurs in a region of the ultraviolet spectrum (280-340 nm), and is relatively free of extraneous radiation. A flowing microwave discharge lamp is used as the source in

this experiment. The measurement is similar to that presented previously by McCullogh [3] and Lempert [4]. Computer programs and several utilities were developed by these investigators.

A microwave-pumped low pressure discharge in argon and water vapor is employed to produce strong OH radical band radiation in the 308 nm region. This radiation is transmitted through the plume and absorption data is taken at various radial positions using an optical multichannel analyzer. This absorption data is then used to compute OH number density using a model for the absorption band characteristics as a function of temperature based on an atlas of line strengths.

Chemical Kinetics of the combustion of propane/air, flow fields, temperature profile, OH number density and water vapor mass fraction distribution, based on the technique of computational fluid dynamics (CFD) have been carried out. Results of CFD computation are compared with that of the experimental observations based on spectroscopic resonance line absorption technique with a good agreement.

II. Experimental Apparatus

A schematic diagram of the instrumental approach is illustrated in Figure 1. Blocks 1, 2, and 3 show the OH lamp, microwave generator and tesla coil, respectively. Blocks 4, 9, and 10 illustrate the propane/air burner, spectrograph,

and spectrum analyzer, respectively. Detailed dimensions of Blocks 1, 2, and 3 in Figure 1 are illustrated in Figure 2. The size of the unit is in mm. We utilize a microwave discharge lamp which consists of a flowing glass tube, water jacket, McCarroll resonance cavity, tesla coil, and ultraviolet (UV) quartz window. This lamp is driven by microwave discharge in water vapor at a pressure of approximately 1 torr. The microwave lamp is driven by a 100 watt microwave generator of adjustable power. A 5000-V DC capillary discharge tube system is also available and has been utilized for some of this work.

A 0.5 meter Czerny-Turner McPherson UV Spectrograph and a 1 meter double-pass J-Y Ramanoor with a Princeton instrument OMA are used which are illustrated in Blocks 9 and 10 of Figure 1. The McPherson instrument can cover the region from 302-318 nm with 500 channels and up to 64 spatial tracks along the slit with an EG&G SIT Vidicon and available memory. The J-Y Ramanoor can acquire a 5 nm wide window of data in the 308 nm region with 700 diode channels in 1 spatial track. The McPherson instrument is utilized to acquire absorption data while the Ramanoor is used for lamp characterization and single line rotational temperature measurements.

A strong OH radical band radiation produced by the microwave discharge lamp in the 308 nm region is transmitted through the plume. The burner is back lighted by an enlarged

image of the OH spatial discharge viewed down the axis of the McCarroll resonance cavity. The back lighted burner image is rotated 90 ^{0} to the spectrometer slit so that the slit forms a radial "slice" through the axisymmetric burner flame. An EG&G Model 1254 axisymmetric Vidicon OMA system is used to acquire OH absorption spectra at 64 distinct spatial tracks along the slit length of the spectrograph. This arrangement allows a zone by zone analysis of transmitted radiation in the axisymmetric burner flame for development of future radial inversion schemes. Thermocouple scans across the plume diameter are used to measure the radial profile of plume temperature. The absorption data are then used to compute OH number density using a model for the absorption band characteristics as a function of temperature based on an atlas of line strengths [5]. Distribution of OH number density and temperature profile across the flame can, thus, be detected.

III. Data Analysis and Model Computation

The technique is based upon the fact that aggregate values for the integrated absorption of the sample within each spectral window can be accurately predicted, and that the temperature dependence of these values is sufficient to yield significant instrumental temperature sensitivity. The spectroscopy of the $2\Sigma^{+} - 2\pi$ OH transition is well known [6]. Generating a surface of absorption values proceeds in the

three steps: (1) Generation of the lamp emission spectrum, (2) calculation of the absorption coefficient for OH as a function of wavelength and temperature, and (3) convolution with the spectrometer bandwidth functions to determine the transmission function through the ratio of the transmitted to the incident intensities. Figure 3 shows the flow chart for the absorption model computation.

By using Voigt profile, Figures 4 and 5 show the intensity distribution of absorption lines for OH as a function of wavelength for temperatures 2400 K and 5000 K, respectively. Figure 6 shows the OH emission spectrum from the microwave lamp based on experimental observation at the translational temperature of 600 K: while Figure 7 depicts that of OH emission spectrum based on model calculation with the procedures described in Figure 3. By using absorption lines for OH at various temperatures, shown in Figures 4 and 5, through the convolution with spectrometer bandwidth function, one can calculate the transmission of microwave lamp radiation with signal center at 309 nm, as shown in Figure 8. Here, N_{OH} denotes the OH number density; and L, the optical path length.

As shown in Figure 1, a thermocouple is used to measure temperature across the flame. The thermocouple is of the Pt-Rh variety, consisting of a bare bead junction exposed to the flame. The leads are bent parallel to the burner flow for one inch upstream of the junction to minimize gradients which

induce conductive losses in the thermocouple leads. The junction temperature is corrected for radiation losses by equating the radiation from the junction surface with the steady-state convective heat transfer from the flame gases. Gas properties are computed using equilibrium CFD results and the calculated gas velocity profile.

With the corrected temperature profile across the flame, one can calculate the OH transmission and OH number density with reference to Figure 8. Figure 9 illustrates OH number density and OH transmission across the flame. It shows clearly that the transmission of UV radiation is lowest at the edge of the flame in which the radius is 2.4 cm, in contrast to the central portion (core) of the flame at which the transmission of UV radiation is highest. It is also shown that OH number density is highest at the edge of the flame and lowest at the core of the flame.

Figure 10 shows the corrected temperature profile across the flame adjusted from the thermocouple measurement. Comparison between Figures 9 and 10 shows that the profile of the OH number density is very much in phase with the temperature profile of flame in which the OH number density dominates at the region with temperature in the range of 1900 to 2050 K.

IV. Computation of Flow Field and Chemistry of Turbulent Propane/Air Flames

The CFD code for combustion turbulent flows, developed by Markatos et al.[7], was used as a base to carry out the present computation. The following modifications were made to the code: (1) the fuel was changed from methane to propane; and (2) the geometry of the burner was modified to fit our present case.

A staggered grid for the velocity components is used in this computer program which was first developed by Harlow and Welch.[8] Figure 11 shows the distribution of grid points for the computation. The baseline horizontal axis indicates the center line of axial coordinate of the burner. A block with cross-hatching lines shows the location of the burner wall. Fuel is injected into the central portion of the burner with a radius of 1 cm, and the remaining outer radius of the burner is injected with the compressed air of two atmospheric pressures.

In order to match the experimental observation, the inlet conditions for the CFD computation are as follows: fuel (propane) flow rate: 1.8×10^{-4} kg/s; air flow rate: 2.5×10^{-4} kg/s; velocity of fuel stream: 28 cm/s; velocity of air stream: 6.5 cm/s; temperature of fuel and air stream: 275 ^{0}K; and inlet pressure : 2 atm.

Figures 12 and 13 show the velocity profiles along axial and radial directions, respectively. The location of the

experimental observation of UV radiation and the thermocouple measurement of temperature across the flame is illustrated with a series of small circles connected by a line. It shows an acceleration of the axial component of the velocity profile at the location of high pressure gradient which is induced by the high combustion rate between fuel and air and input compressed air and fuel. As to the radial component of the velocity profile, it shows that air flows toward (negative direction) the central core (fuel) of the burner; while fuel flows toward (positive direction) the outer radius (air) of the burner during the period of combustion inside the burner. Outside the exit of the burner, it also shows that air, surrounding the burner, flows toward the flame mixing with the jet stream resulting from combustion.

Figure 14 shows the temperature profile based on CFD computation. This figure shows that there is a peak temperature located at the boundary surrounding between fuel and air at the initial stage of combustion inside the burner. This high peak of temperature profile moves gradually outward toward the radial direction, and decreases suddenly outside the edge of the flame after the flow passes through the exit of the burner. This cylindrical-like high peak of temperature profile disperses gradually toward both inward and outward of radial directions as it flows away from the exit of the burner.

The temperature profile based on CFD computation is compared with that measured by thermocouple across the flame. Figure 10 shows the comparison with a good agreement. However, CFD computation is based on an axisymmetric model; while in reality, the measurement is an asymmetric profile.

In the consideration of hydrocarbon oxidation, the following four-step scheme proposed by Hautman et al.[9] is employed:

$$C_xH_y \rightarrow C_xH_{y-2} + H_2$$

$$C_xH_{y-2} + \frac{x}{2} O_2 \rightarrow xCO + \frac{y-2}{2} H_2$$

$$CO + \frac{1}{2} O_2 \rightarrow CO_2$$

$$H_2 + \frac{1}{2} O_2 \rightarrow H_2O$$

In order to reduce computer time, the partial equilibrium assumption has been used.[10] This involves the assumption that the following four bimolecular reactions are equilibrated:

$$H + O_2 \rightleftharpoons OH + O_2$$

$$O + H_2 \rightleftharpoons OH + H$$

$$OH + OH \rightleftharpoons H_2O + O$$

$$CO + OH \rightleftharpoons CO_2 + H$$

This assumption reduces the number of kinetic equations to be

solved. In this paper, both OH and H_2O density profiles will be illustrated from the CFD computation.

The OH number density profile across the flame is compared with results obtained from CFD computation and with the results from the UV radiation observation. Figure 15 shows these comparisons of OH number density profiles with a good agreement. The conclusions drawn for temperature profiles of symmetric and asymmetric shapes, shown in Figure 10, are also true in this case of OH number density profiles between CFD computation and experimental measurement.

Figure 16 shows OH number density (in terms of mass fraction, in g/g) distribution in the whole flow field based on CFD computation. It clearly shows that OH radicals are produced at the interface between fuel and air at the beginning stage of combustion. This peak profile of OH number density gradually propagates outward toward the edge of the flame outside the exit of the burner, as shown in Figure 9, observed from the UV radiation experiment. The maximum value of OH number density is located at the exit of the burner and decreases gradually as it flows away from the exit.

Figure 17 shows water vapor (H_2O) number density (in terms of mass fraction, in g/g) distribution in the whole flow field based on CFD computation. Results show that high peaks of H_2O are produced near the boundary surrounding between the fuel and air at the initial stage of combustion inside the burner which is very similar to the temperature profile.

Again, this high peak of H_2O density distribution disperses toward the inward and outward direction of the flame axis as it flows away from the exit of the burner.

V. Conclusion and Discussion

In this study, determination of the OH radical based on spectroscopic techniques has been carried out. Mathematical models for the transport of the lamp characteristic spectrum through flame gases have been used to compute Voigt line profiles. We have utilized these models, developed by McCullogh [3,5] and Lempert [4], for inversion of off diameter scans of wavelength data in the region of 306-318 nm of OH radiation to total OH number density profiles. These models utilize a low pressure OH lamp as a source for an absorption measurement.

A thermocouple is used to measure temperature across the flame. The measured temperature data from the thermocouple are corrected for radiative losses using the equilibrium computation of gas properties based on CFD code.

CFD code for combustion turbulent flows has been used to compute flow field, temperature profile and OH number density distribution. Comparison between experimental observation and CFD computation shows a reasonably good agreement.

Acknowledgement

The authors appreciate the support of the present study through NASA Grant NAG8-102. They are also indebted to B. B. Barrontine of the University of Alabama in Huntsville for his help in carrying out the experimental observation.

References

1. Gaydon, G. H., The Spectroscopy of Flames, John Wiley and Sons, New York, 1957, pp. 1-279.
2. Neer, M. E., "Numerical Calculation of UV Emission and Absorption Spectra of OH" for Aerospace Research Laboratories, Wright-Patterson AFB, Ohio, ARLTR 74-0109, August 1974, pp. 1-147.
3. McCullough, R. W., and Northam, G. B., "A High Speed Non-Instrusive Temperature Diagnostic for Combustion Processes", Aeronautical Research Associates of Princeton, Inc., A.R.A.P. Tech Memo 82-4, presented at The Joint Army-Navy-NASA-Air Force Combustion Meeting, Vol. 1, 1982, pp. 435-457.
4. Lempert, W. R., "Microwave Resonance Lamp Absorption Technique for Measuring Temperature and OH Number Density", NASA Langley Research Center, 1987, pp. 1-21.
5. McCullogh, R. W., "Improvements to the NASA OH Temperature Measurement System," ARAP Report No. 548, Final Report for Contract NAS1-14853, NASA Langley Research Center, April 1985, pp. 1-113.
6. Dieke, G. H., and Crosswhite, H. M., "The Ultraviolet Bands of OH", J. Quant. Specrosc. Radiat. Transfer, Vol. 2, 1962, pp. 97-199.
7. Markatos, N. C., Spalding, D. B., and Srivatsa, "Prediction of Hydrodynamics and Chemistry of Confined Turbulent Methane-Air Flames in Two Concentric Tube

Combustor", NASA CR-135412, June 1978, pp. 1-284.

8. Harlow, F. H., and Welch, J. E., "Numerical Calculation of Time-Dependent Viscous Incompressible Flow of Fluid with Free Surface", Physics of Fluids, Vol. 8, 1965, pp. 2182-2189.

9. Hautman, D. J., Dryer, F. L., Schug, K. P., and Glassman, I., "A Multiple-Step Overall Kinetic Mechanism for Oxidation of Hydrocarbons," Combustion Science Technology, 1981, pp. 219-235.

10. Srivatsa, S. K., "Combustions of Soot and NO_x Emissions from Gas Turbine Combustors," NASA Contract Report CR-167930, May 1982, pp. 1-322.

Figure Captions

Figure 1 Block diagram for the experimental setup of spectroscopic observation of OH radicals.

Figure 2 Detailed dimensions of OH lamp, microwave generator, tesla coil and UV quartz window. The size of the unit is in mm.

Figure 3 Flow chart for the OH absorption model computation.

Figure 4 Intensity distribution of absorption lines for OH as a function of wavelenth for temperature = 2400 K.

Figure 5 Intensity distribution of absorption lines for OH as a function of wavelength for temperature = 5000 K.

Figure 6 OH emission spectrum from the microwave lamp based on experimental observation at the translational temperature of 600 K.

Figure 7 OH emission spectrum from the microwave lamp based on model computation at the translational temperature of 600 K.

Figure 8 Transmission of microwave lamp radiation with signal center at 309 nm as a function of OH radical number density and temperature.

Figure 9 OH radical number density and transmission across the flame from experimental observation.

Figure 10 Corrected temperature profile across the flame

adjusted from the thermocouple measurement (solid line) in comparison with that computed from CFD model (hidden line).

Figure 11 Distribution of grid points for axisymmetric model of CFD computation.

Figure 12 Axial component velocity profile based on CFD computation.

Figure 13 Radial Component velocity profile based on CFD computation.

Figure 14 Temperature profile of the whole flow field based on CFD computation .

Figure 15 OH number density profiles across the flame based on experimental observation (solid line) and on CFD computation (hidden line).

Figure 16 OH number density distribution over the whole flow field based on CFD computation.

Figure 17 Water vapor (H_2O) density profile of the whole flow field based on CFD computation.

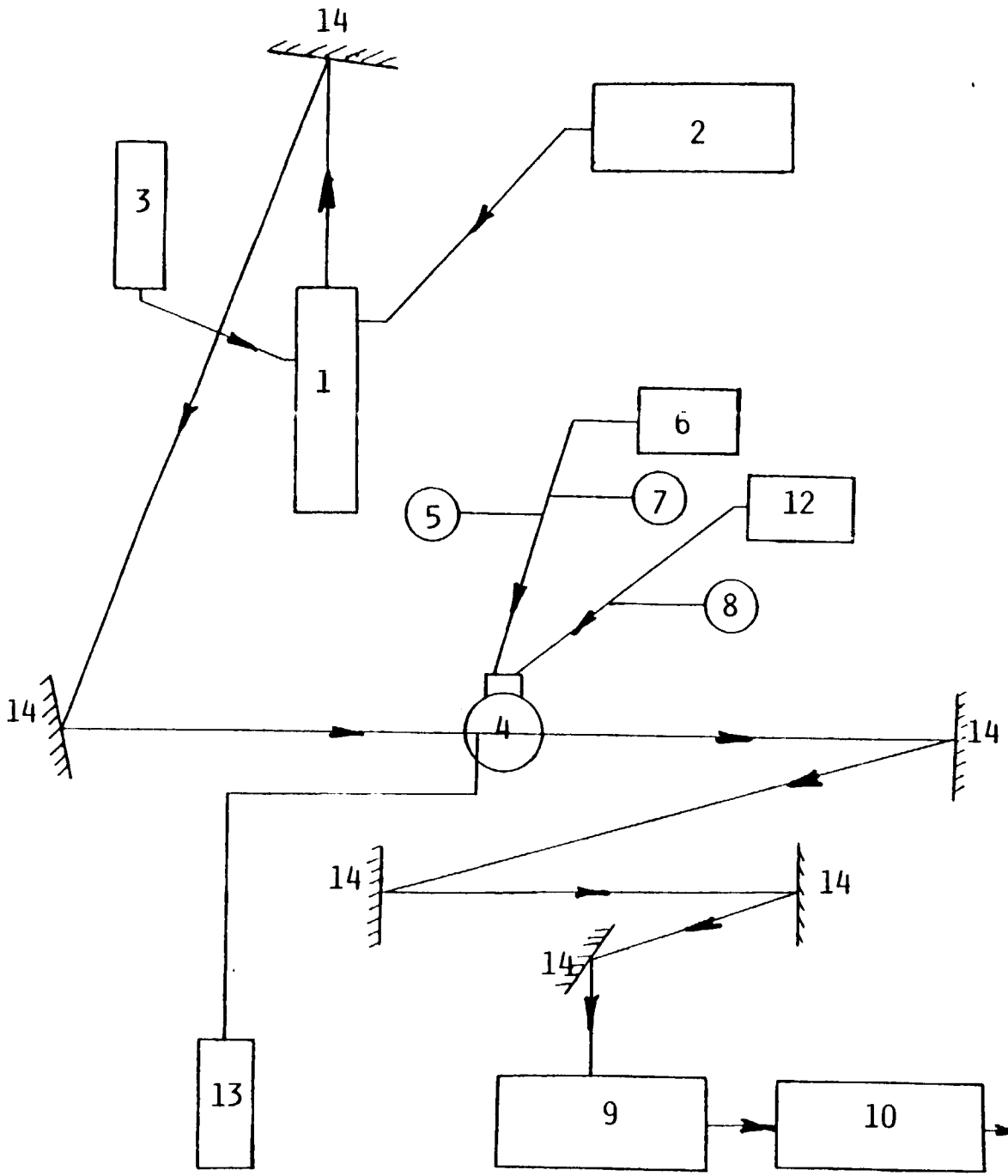

Item	Description
1	OH Lamp
2	Microwave Generator
3	Tesla Coil
4	Burner
5	Pressure Gage
6	Propane
7	Flow Meter (Fuel)
8	Flow Meter (Air)
9	Spectrograph
10	Spectrum Analyzer
11	Personal Computer PC/AT
12	Air
13	Thermometer
14	Mirror

Fig.1

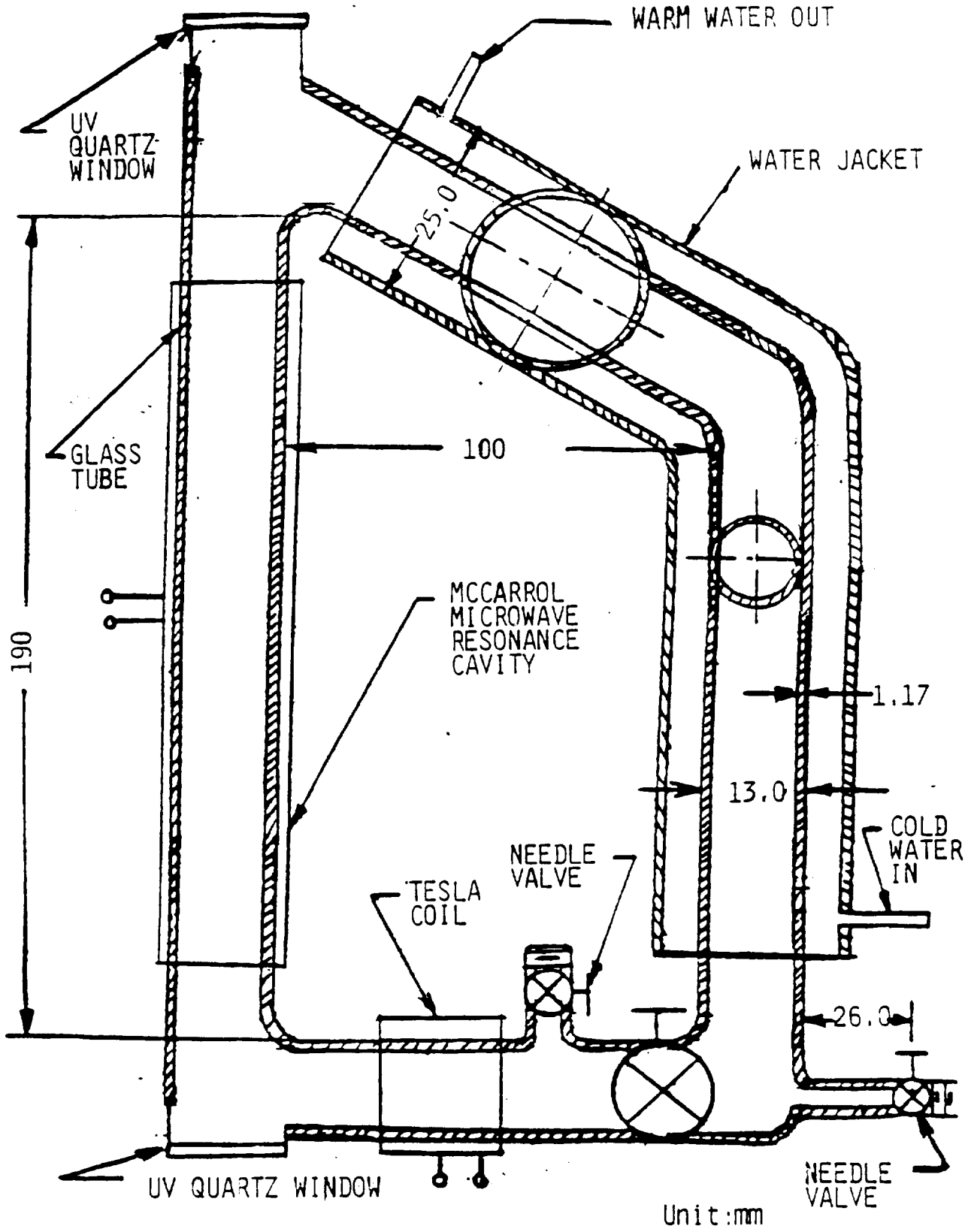
WARM WATER OUT
UV
QUARTZ
WINDOW
WATER JACKET
25.0
GLASS
TUBE
100
190
MCCARROL
MICROWAVE
RESONANCE
CAVITY
1.17
13.0
COLD
WATER
IN
NEEDLE
VALVE
TESLA
COIL
26.0
UV QUARTZ WINDOW
NEEDLE
VALVE
Unit:mm

Fig.2

Flow Chart for OH Absorption Model Computation

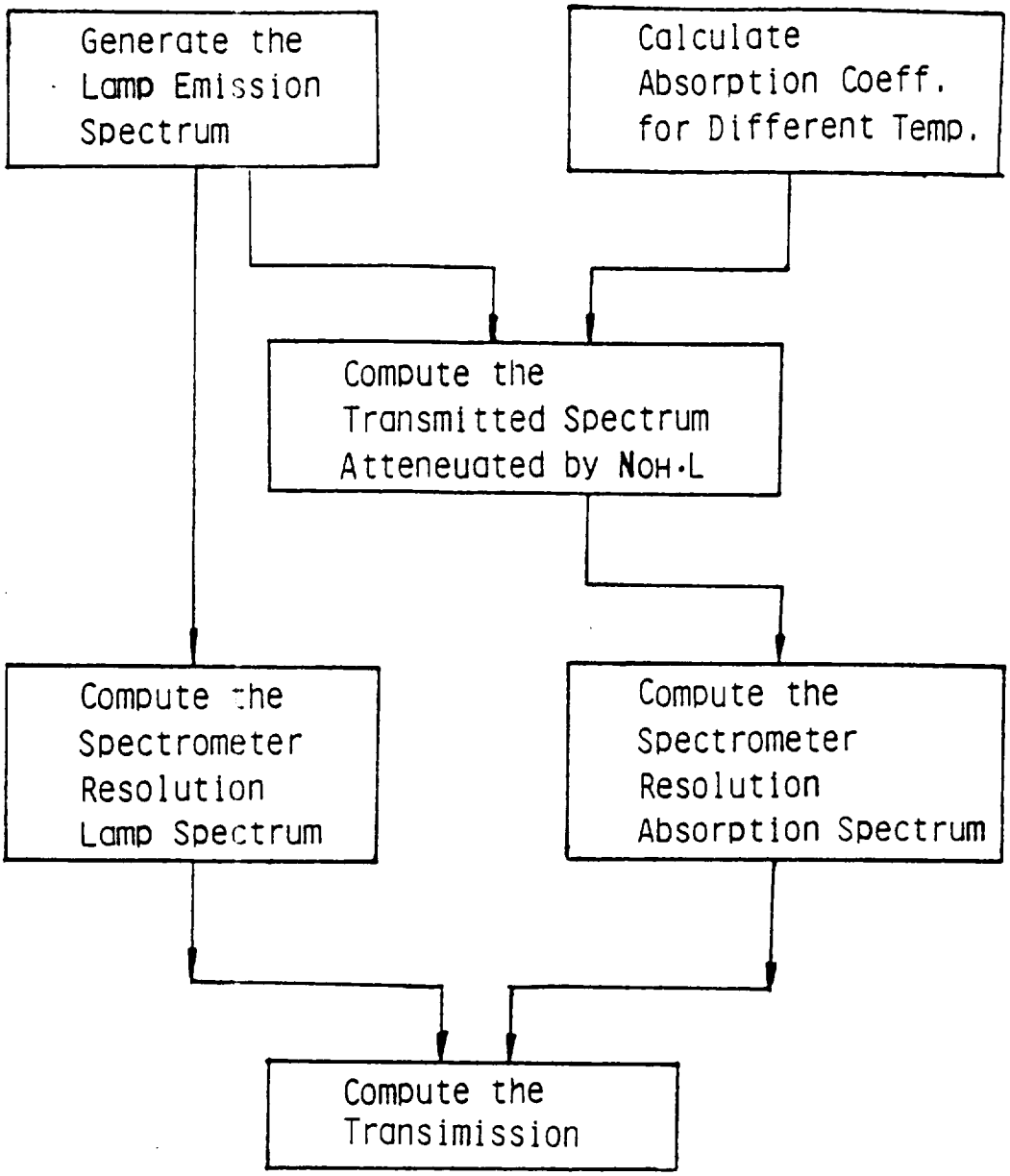

Fig. 3

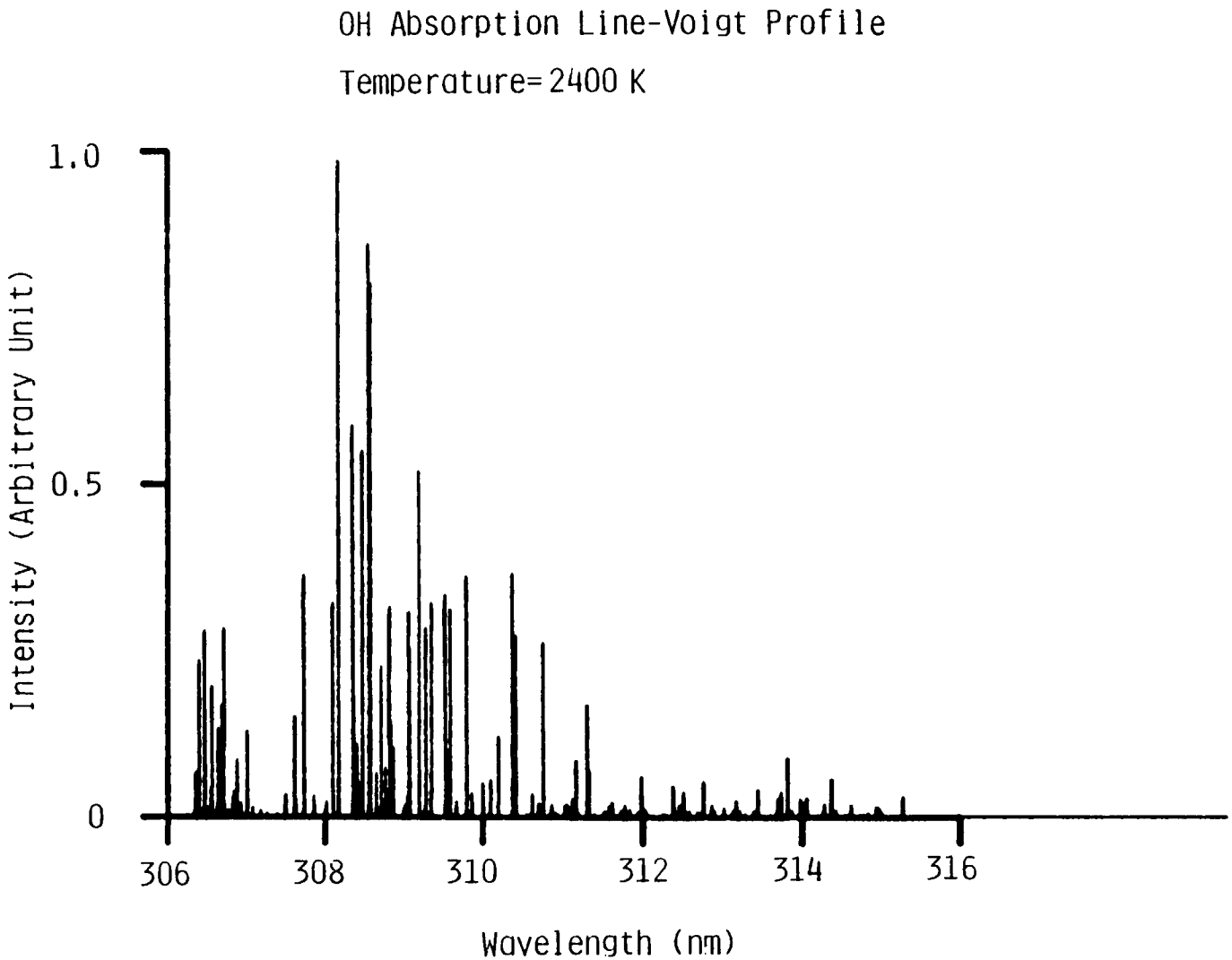
OH Absorption Line-Voigt Profile
Temperature= 2400 K
1.0
0.5
0
Intensity (Arbitrary Unit)
306
308
310
312
314
316
Wavelength (nm)

Fig. 4

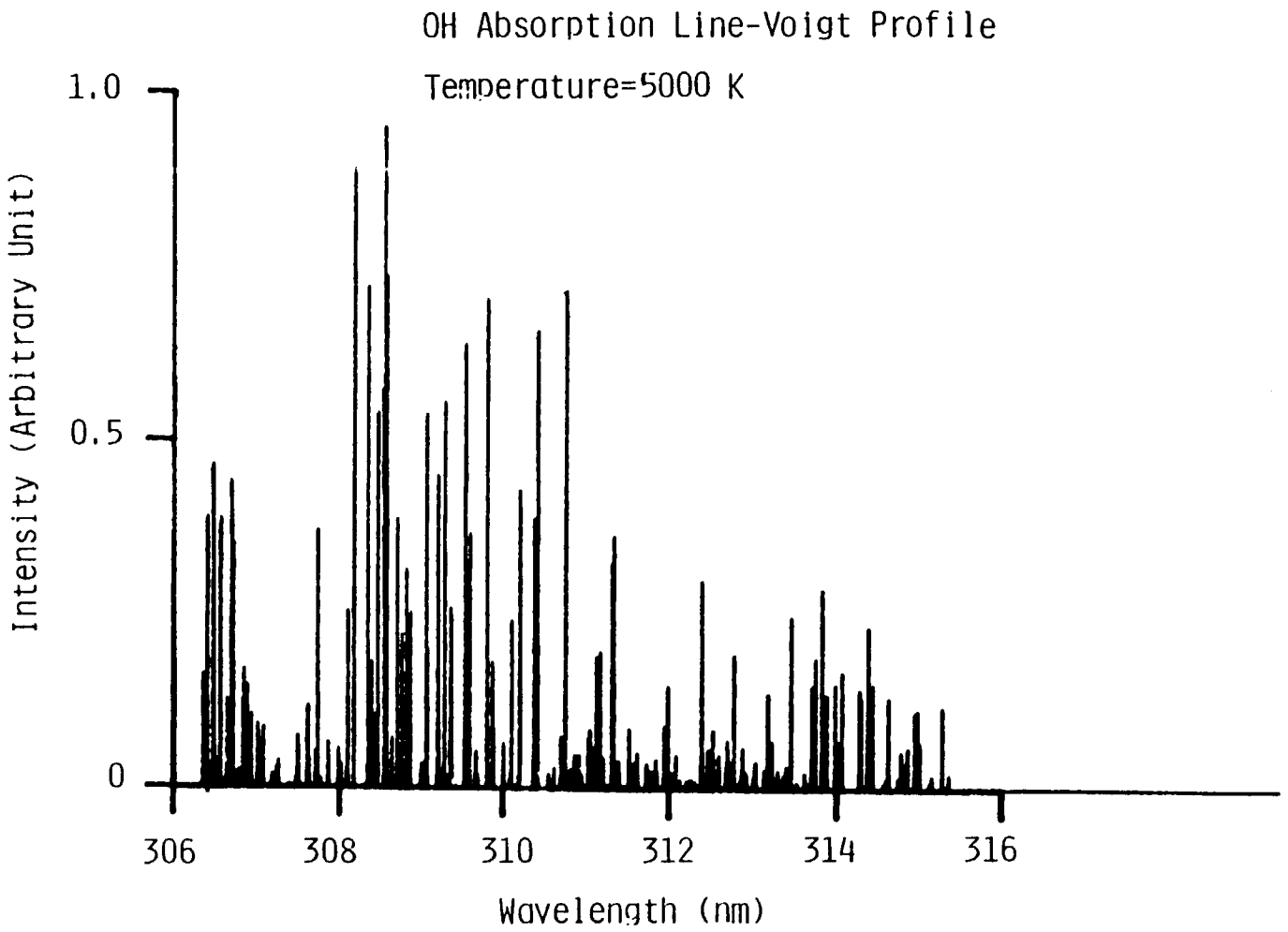
OH Absorption Line-Voigt Profile
Temperature=5000 K
1.0
0.5
0
Intensity (Arbitrary Unit)
306
308
310
312
314
316
Wavelength (nm)

Fig. 5

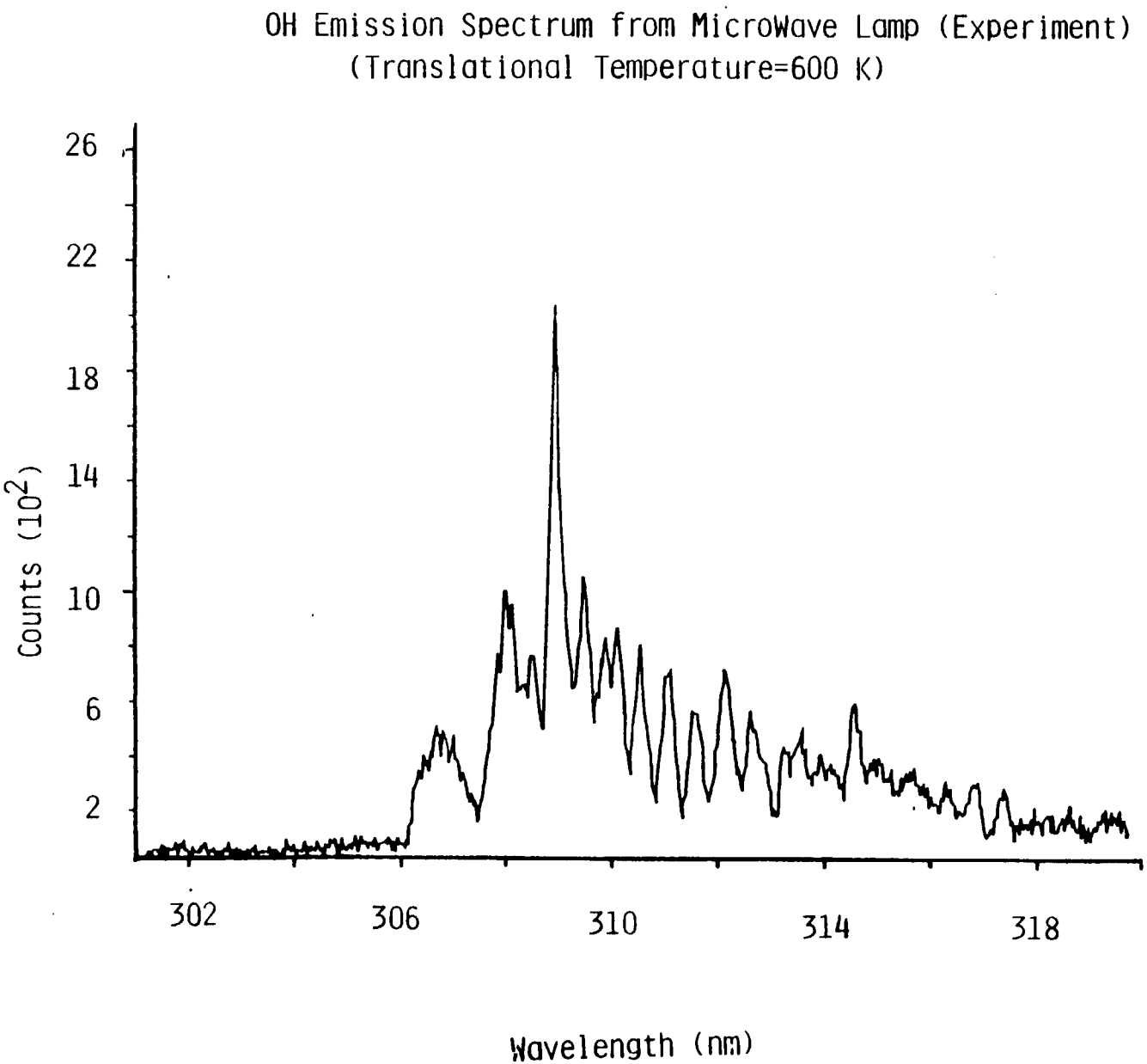
OH Emission Spectrum from MicroWave Lamp (Experiment)
(Translational Temperature=600 K)
26
22
18
14
10
6
2
Counts (10^2)
302
306
310
314
318
Wavelength (nm)

Fig. 6

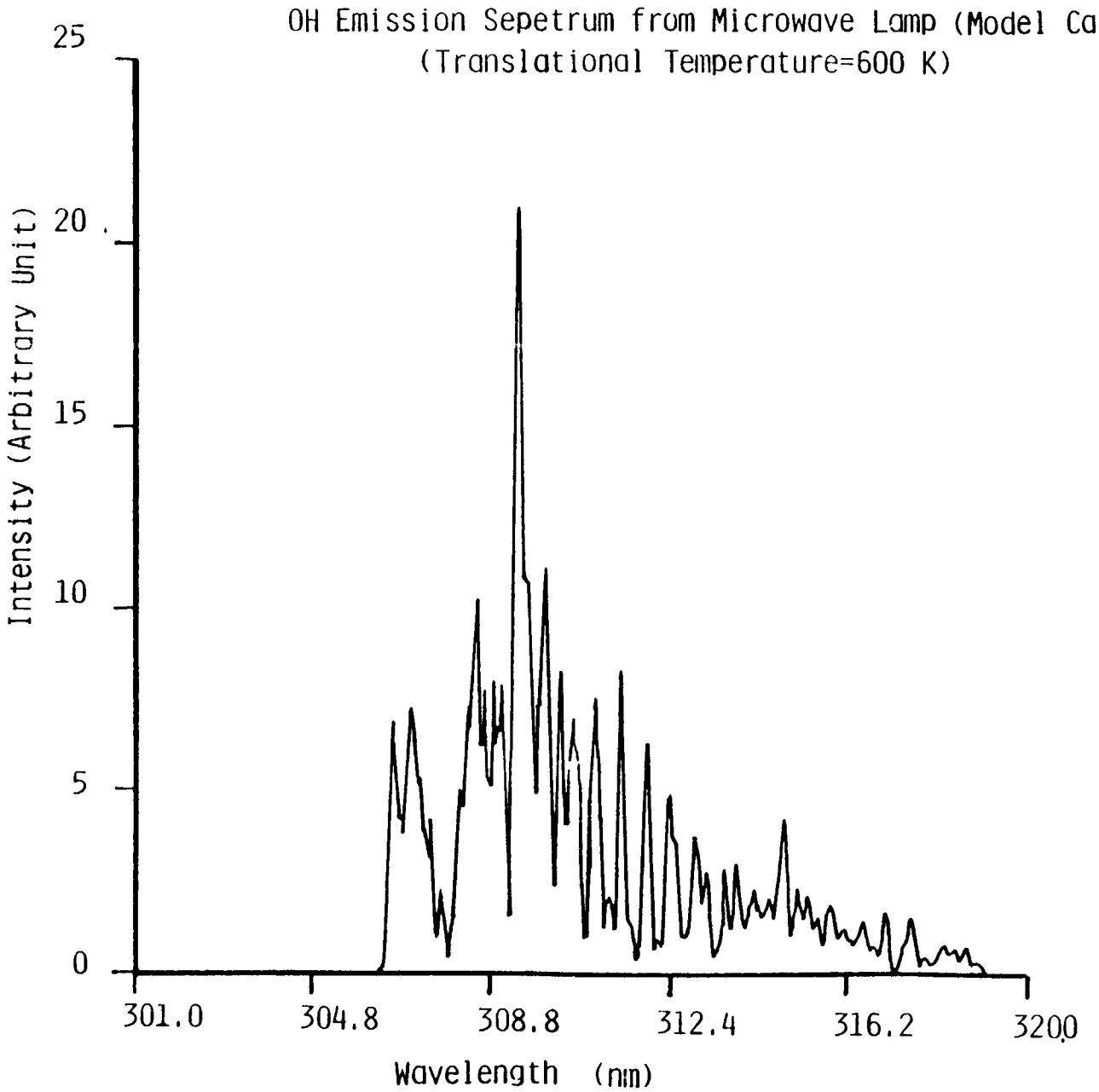
OH Emission Sepetrum from Microwave Lamp (Model Calculation)
(Translational Temperature=600 K)
Intensity (Arbitrary Unit)
25
20
15
10
5
0
301.0
304.8
308.8
312.4
316.2
320.0
Wavelength (nm)

Fig.7

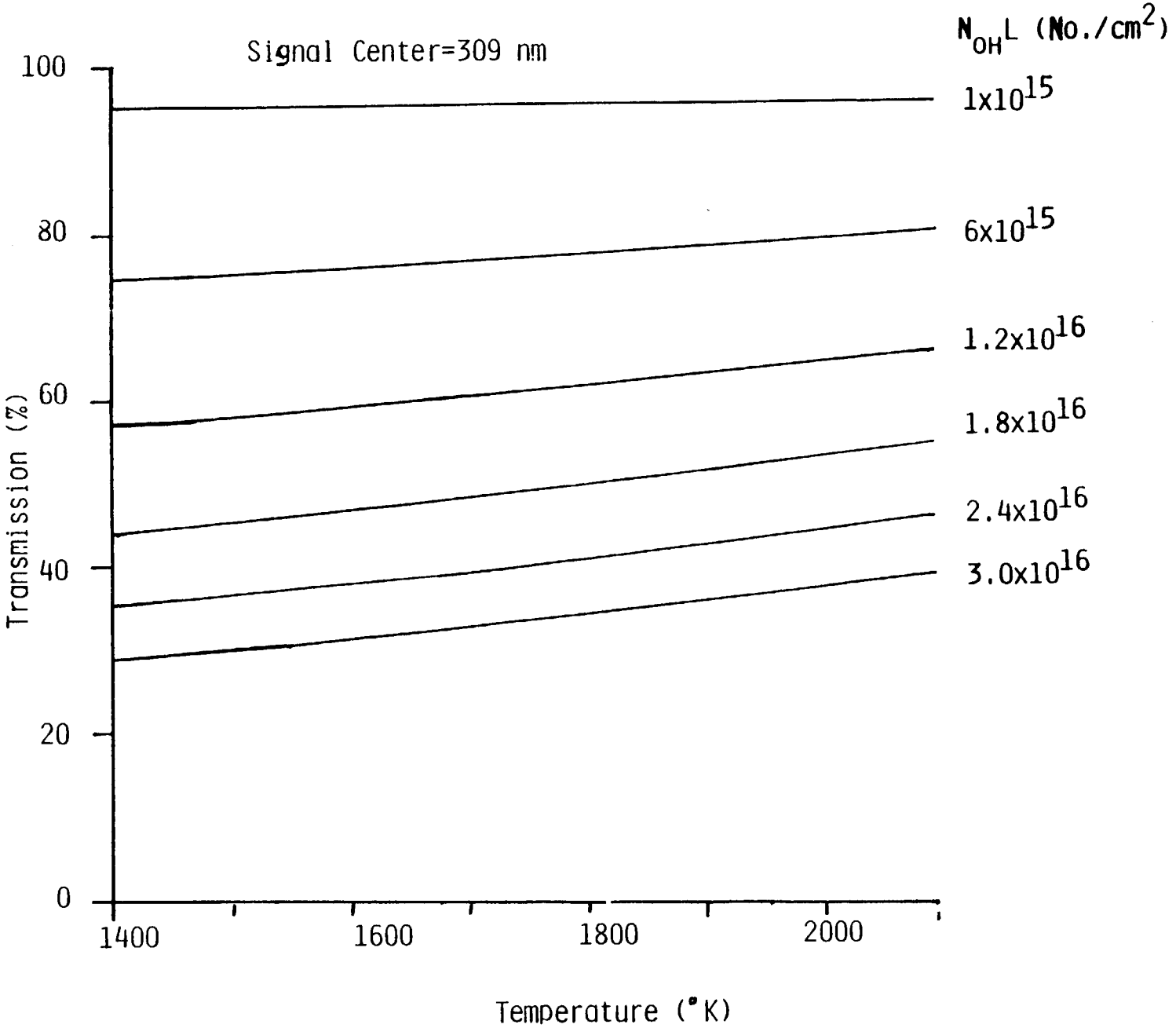
Signal Center=309 nm
$N_{OH}L$ (No./cm^2)
100
80
60
40
20
0
Transmission (%)
1400
1600
1800
2000
Temperature (°K)
1x10^{15}
6x10^{15}
1.2x10^{16}
1.8x10^{16}
2.4x10^{16}
3.0x10^{16}

Fig. 8

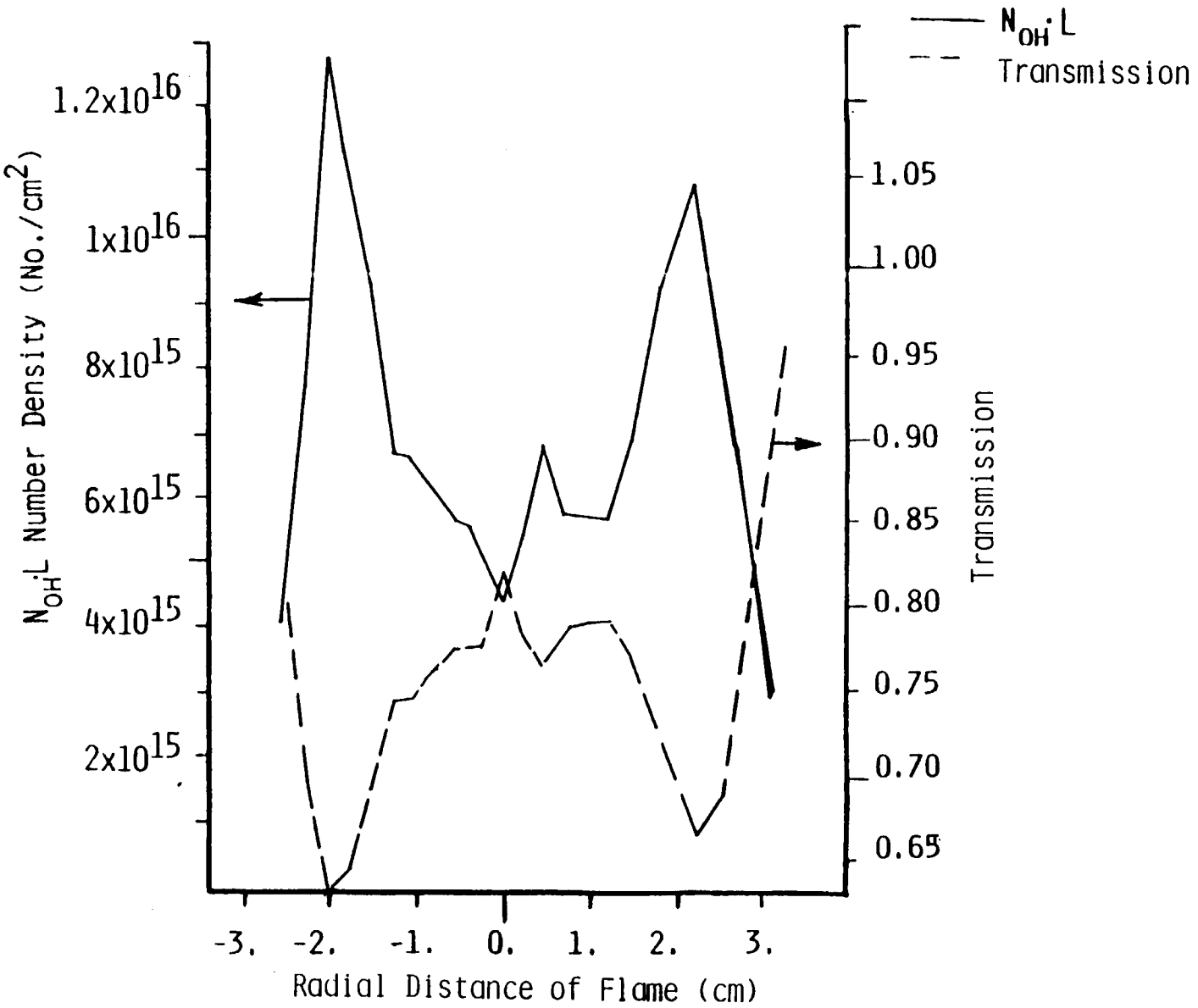
N_{OH}·L
Transmission
N_{OH}·L Number Density (No./cm^2)
1.2x10^{16}
1x10^{16}
8x10^{15}
6x10^{15}
4x10^{15}
2x10^{15}
1.05
1.00
0.95
0.90
0.85
0.80
0.75
0.70
0.65
Transmission
-3.
-2.
-1.
0.
1.
2.
3.
Radial Distance of Flame (cm)

Fig.9

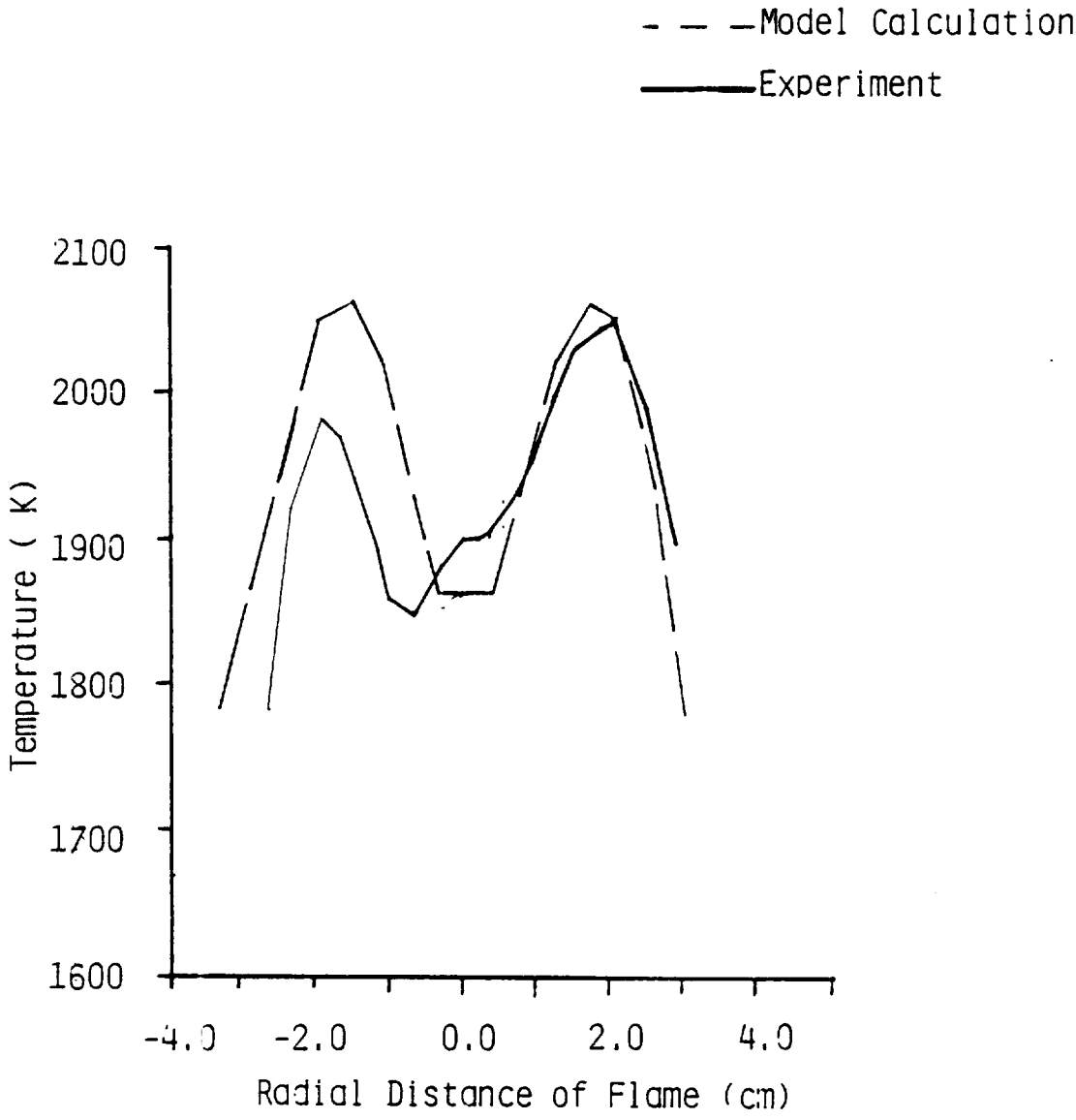
- — —Model Calculation
———Experiment
2100
2000
1900
1800
1700
1600
Temperature (K)
-4.0
-2.0
0.0
2.0
4.0
Radial Distance of Flame (cm)

Fig. 10

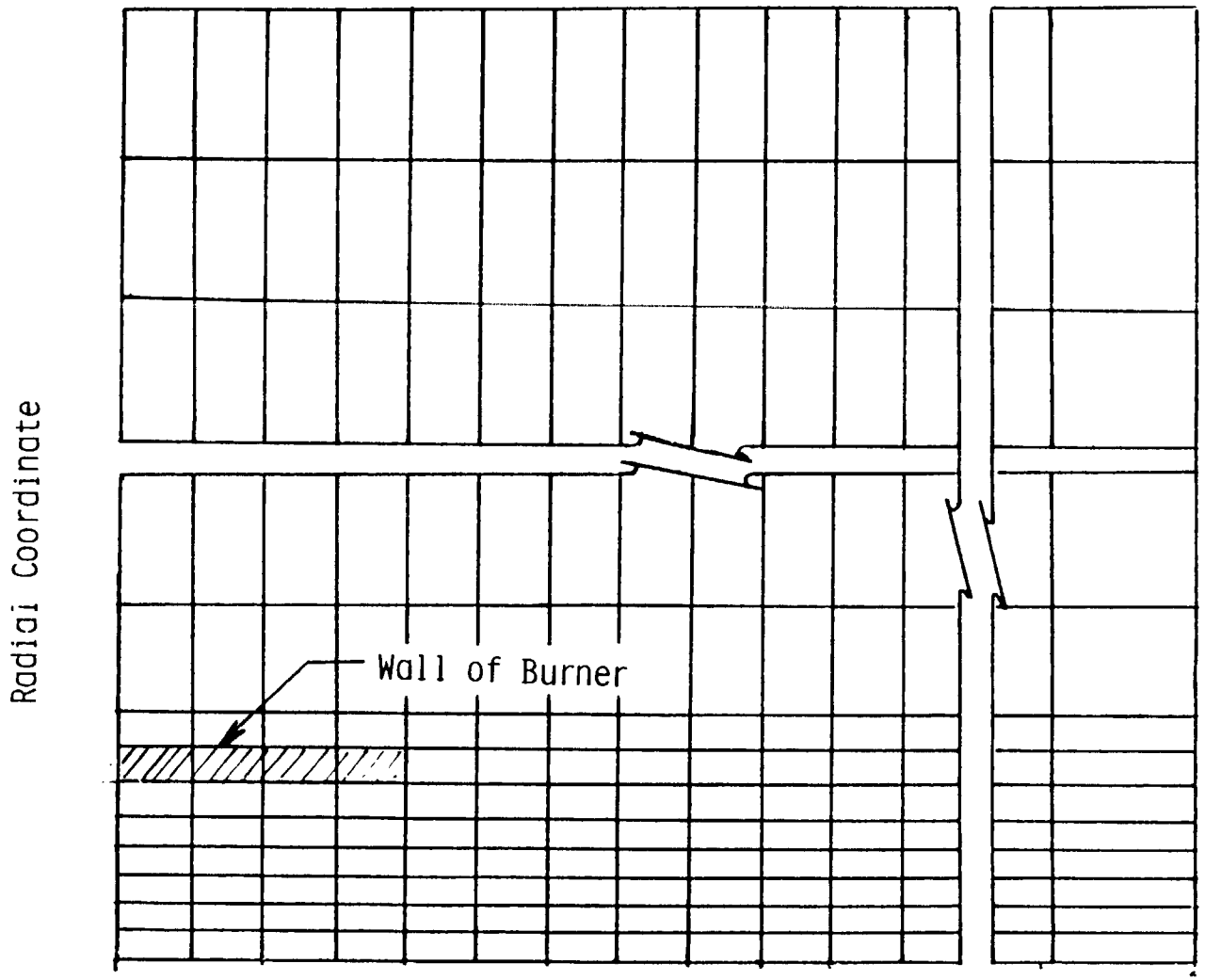

Fig. 11

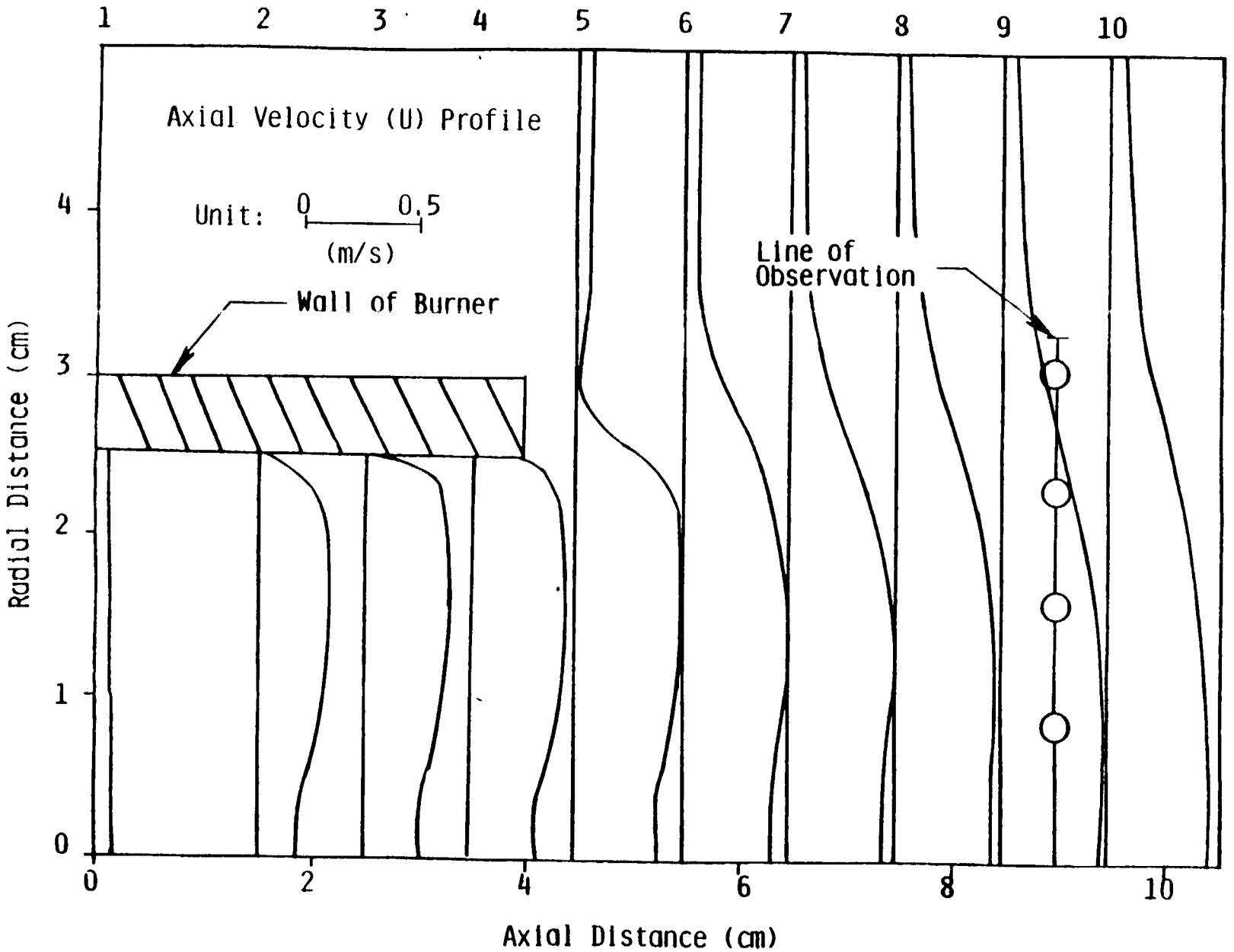
Axial Velocity (U) Profile
Unit: 0 0.5
(m/s)
Wall of Burner
Line of Observation
Radial Distance (cm)
Axial Distance (cm)
0
1
2
3
4
0
2
4
6
8
10

Fig.12

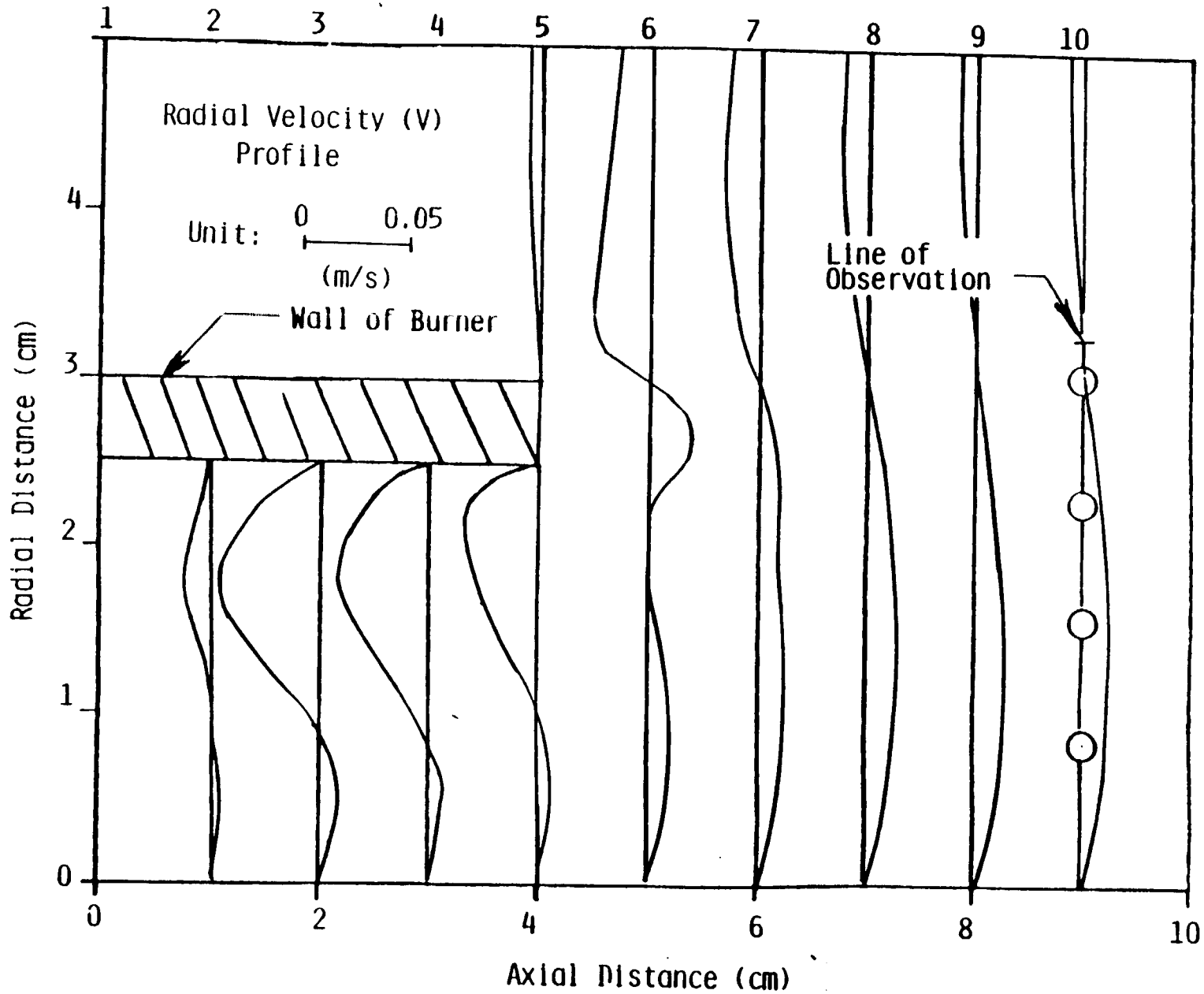
Radial Velocity (V)
Profile
Unit: 0 0.05
(m/s)
Wall of Burner
Line of
Observation
Radial Distance (cm)
Axial Distance (cm)
0
1
2
3
4
0
2
4
6
8
10
1
2
3
4
5
6
7
8
9
10

Fig.13

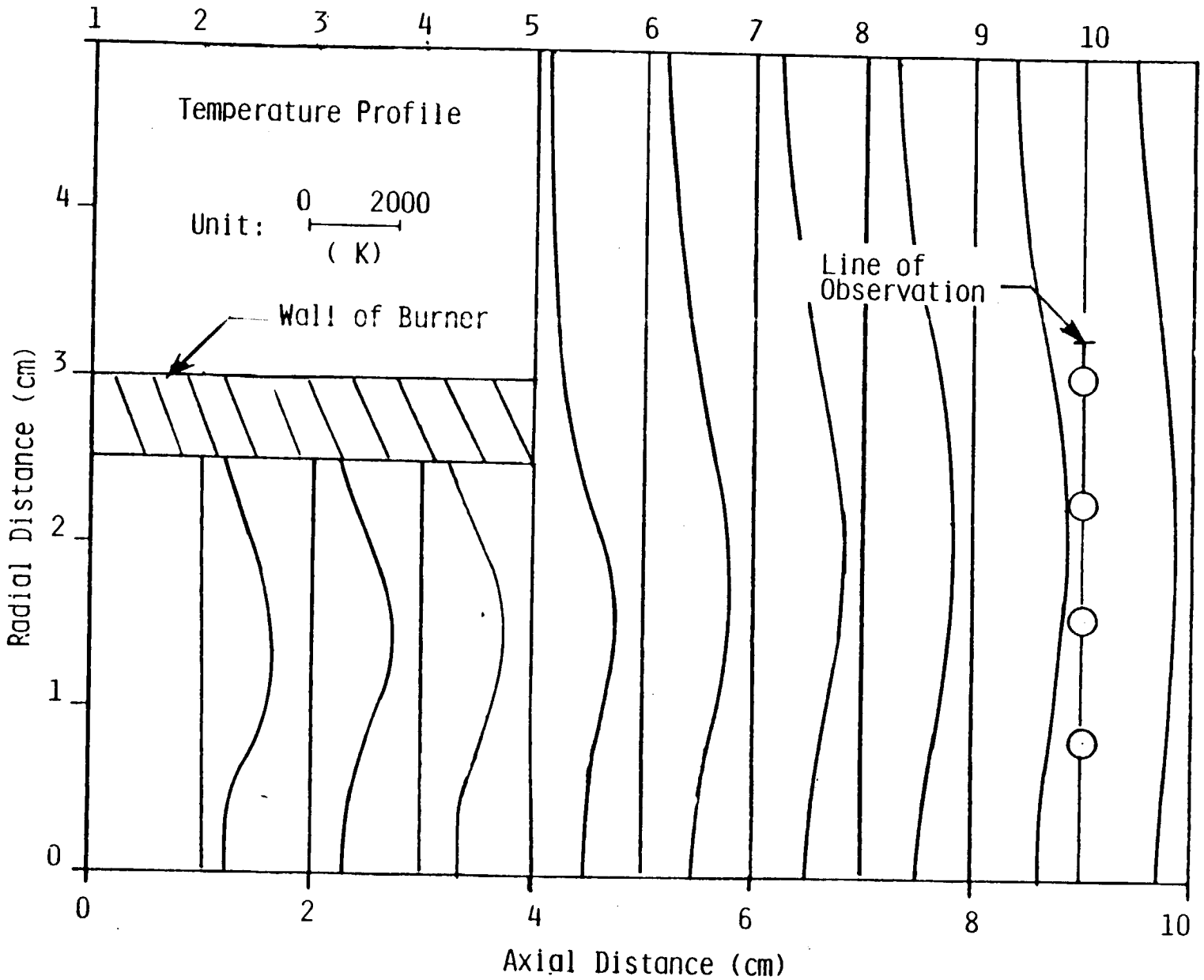
Temperature Profile
Unit: 0 2000
(K)
Wall of Burner
Line of Observation
Radial Distance (cm)
Axial Distance (cm)
0
1
2
3
4
5
6
7
8
9
10

Fig.14

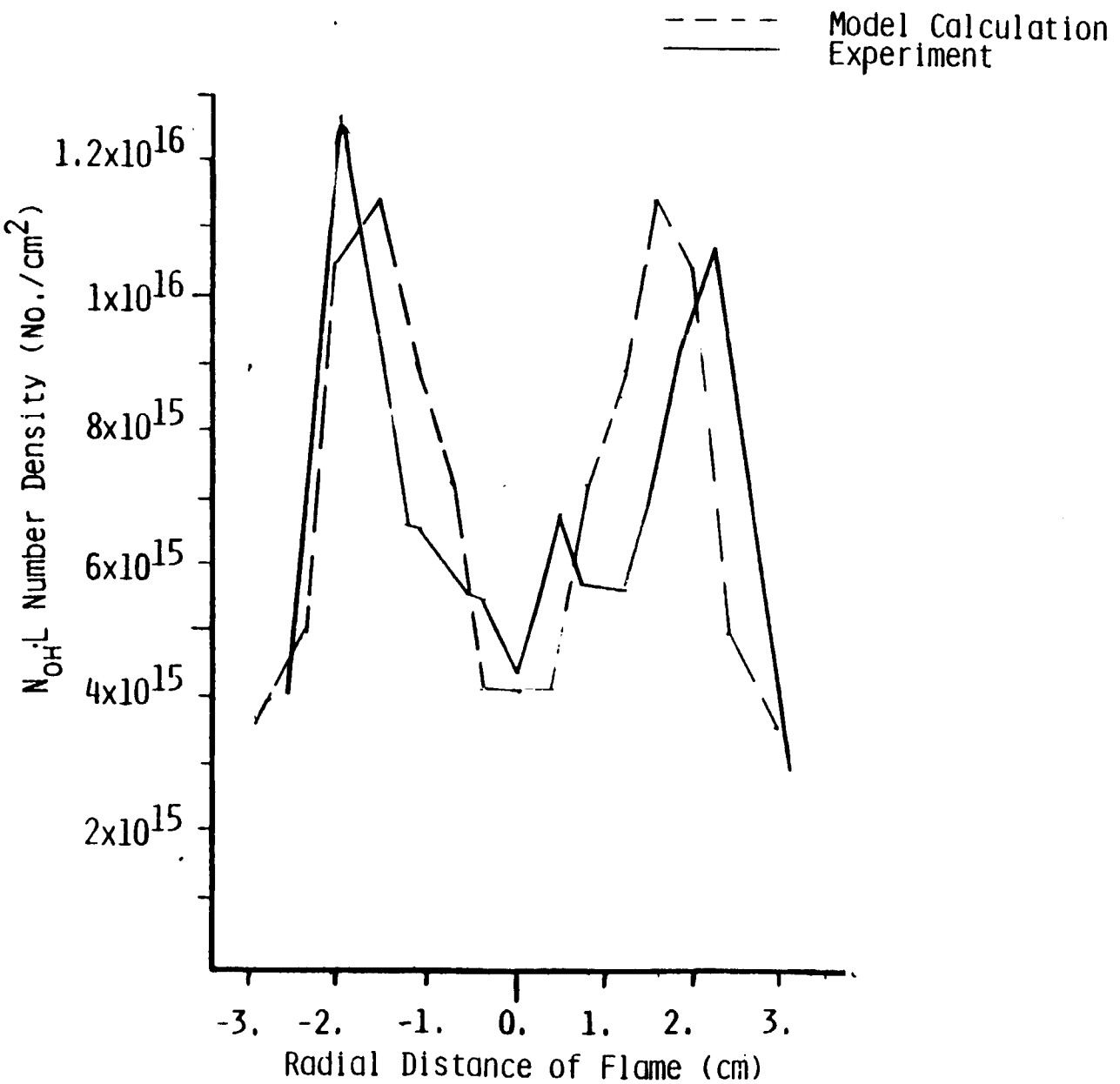
Model Calculation
Experiment
N_{OH}L Number Density (No./cm^2)
1.2x10^{16}
1x10^{16}
8x10^{15}
6x10^{15}
4x10^{15}
2x10^{15}
-3.
-2.
-1.
0.
1.
2.
3.
Radial Distance of Flame (cm)

Fig.15

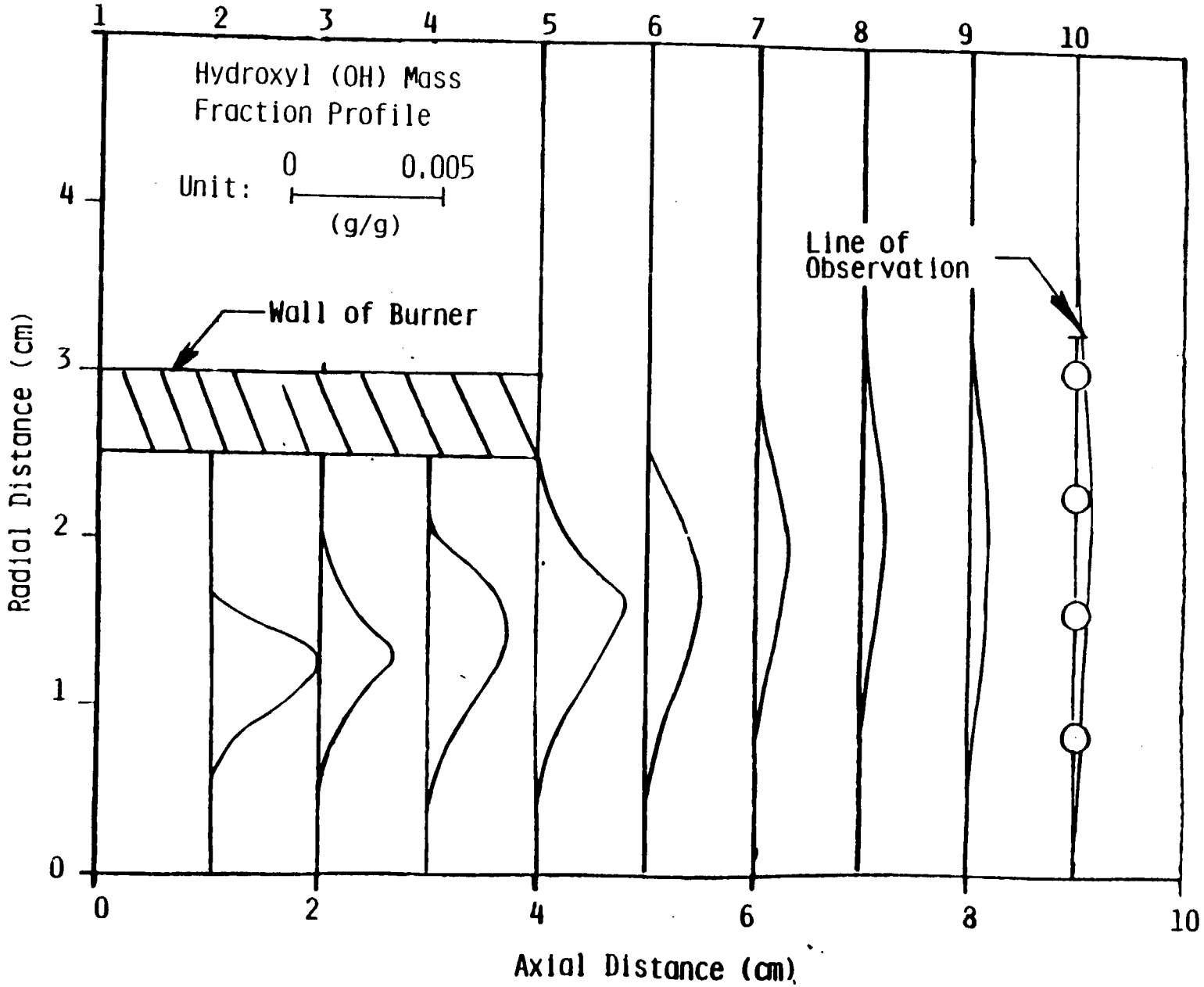
Hydroxyl (OH) Mass
Fraction Profile
Unit: 0 0.005
(g/g)
Wall of Burner
Line of
Observation
Radial Distance (cm)
Axial Distance (cm)
0
1
2
3
4
0
2
4
6
8
10
1
2
3
4
5
6
7
8
9
10

Fig.16

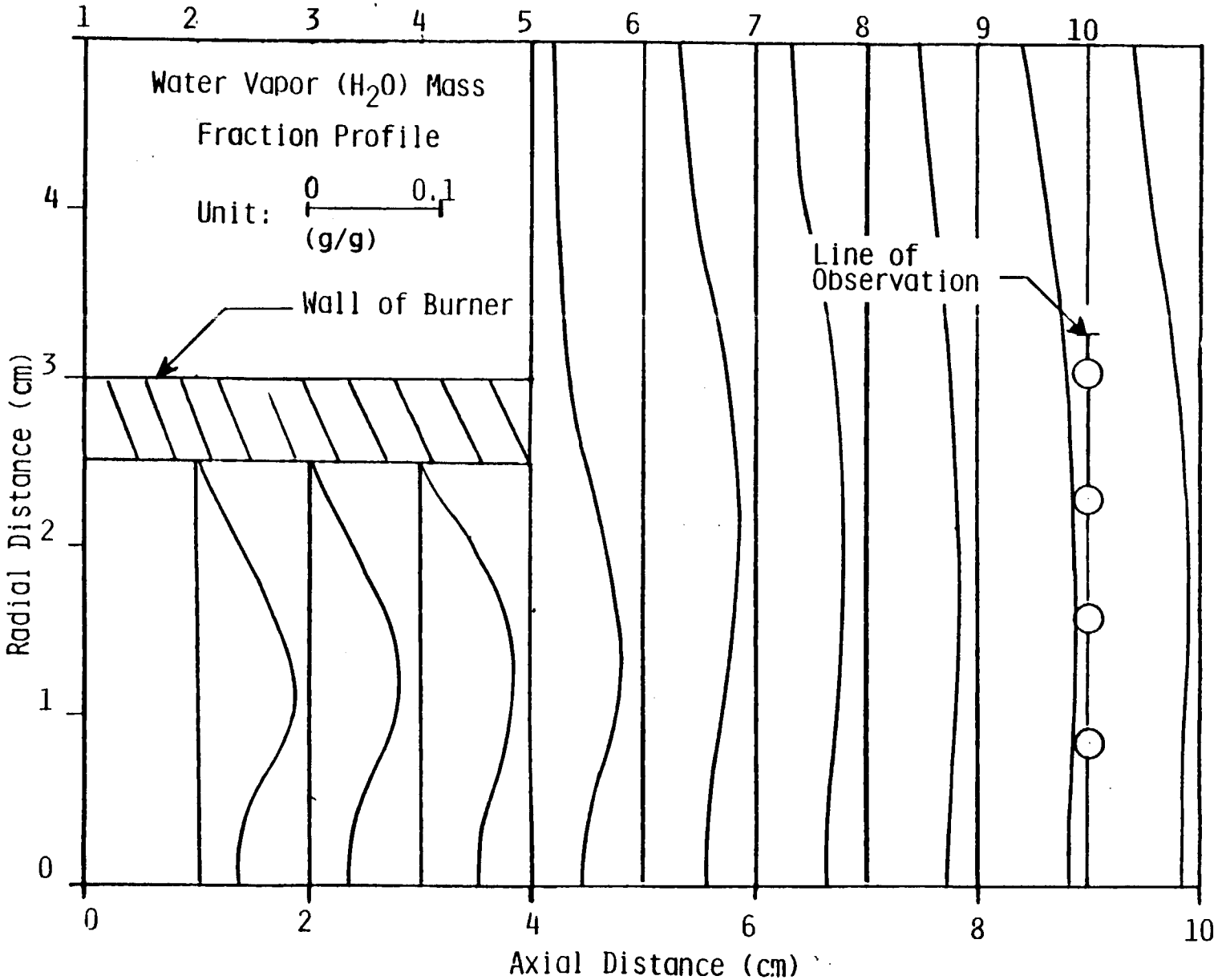
Water Vapor (H_2O) Mass Fraction Profile
Unit: 0 0.1 (g/g)
Wall of Burner
Line of Observation
Radial Distance (cm)
Axial Distance (cm)
0
1
2
3
4
0
2
4
6
8
10

Fig.17